Formation of pillared arrays by anodization of silicon in the boundary transition region: an AFM and XRD study

Serghei K. Lazarouk[a] and Anthony A.G. Tomlinson*[b]

[a]*Byelorussian State University of Informatics and Electronics, P. Brovka 6, Minsk, Belarus*
[b]*Institute of Materials Chemistry, Area della Ricerca di Roma, C.N.R., C.P.10 Monterotondo Staz., 00016 Rome, Italy*

The anodization of Si ⟨100⟩ and ⟨111⟩ wafers in dilute HF solutions has been investigated, with particular reference to probing the surface chemistry and features between the porous and electropolishing regions (the 'boundary transition' region). Conditions have been found for inducing the formation of ordered arrays of columnar (or 'pillar') artefacts, shown to occur only in this region, and whose formation depends crucially on electrochemical parameters and anodization times. Detailed atomic force microscopy (AFM) observations confirm this suggestion, and demonstrate that the arrays consist of relatively ordered long grooves and trenches, though the pillars forming them vary greatly in size. AFM also shows that the best anodization time for maximum ordering of these arrays is *ca.* 12 min, both low (4 min) and high (40 min) anodization times giving rise only to disordered surface structures (though still columnar even after 40 min). These arrays form pseudo-planes which attenuate the absorption of X-rays by (111) and (100) reflections, whereas the non-pillared ones do not. Relevance to current pore formation theories is discussed.

The rediscovery of photoluminescence in porous silicon by Canham in 1990[1] led to a boom in the research literature of investigations aimed at clarifying pore formation mechanism(s).[2] In most reports, the major concern has been with formation of a labyrinth of interpenetrating pores,[3] and more recently the use of supercritical fluids has allowed porosities beyond 95% to be attained.[4] Despite these advances in increasing porosization and its relationship to luminescent characteristics, there has been less interest in determining the range of experimental conditions leading to organisation of surface arrays. As part of a long-standing interest[5] in fine-tuning luminescence characteristics through the various regions (electropolishing, porous and transition regions[2]) it has been found recently that working in the boundary transition region (*i.e.* between the porous and transition regions of ref. 2) amorphous Si deposited on alumina templates can give rise to photoluminescent columnar surface artefacts ('pillars').[6] Subsequently, we found both Si(111) and Si(100) crystal surfaces can also give rise to pillar-type artefacts and that these are oriented in arrays in such a way as to cause anomalous X-ray diffraction effects.[7]

We here give more details on the preparation conditions necessary for obtaining such structures, which are shown to lie close to the boundary transition region (with or without light stimulation). The organisation of the surface artefacts is examined utilising AFM (atomic force microscopy).

Experimental

Materials and electrochemistry

All n and p-doped Si ⟨100⟩ and ⟨111⟩ wafers were commercial Czochralski-grown samples having resistivities of 4.5–0.01 Ω cm, and were used as received.

The cell for anodic etching was of a conventional design consisting of a PTFE sleeve (i.d. 1.6 cm) attached to a silicon wafer (4 cm diameter) containing an aluminium sample holder which also acted as an anode (Fig. 1). The cathode was a Pt (or Nb) wire and the reference electrode a Pt ring. Typically, anodisation of each Si wafer was carried out in a HF solution with an anodic current of 1–20 mA cm^{-2} for 1–40 min. Typical anodization conditions were: 1–40% *m/m* aqueous solution of HF acid at a constant current density, as controlled by a potentiostat. Anodization was also performed under light from a 100 W tungsten lamp placed at 15 cm from the sample. The thickness of films was measured using SEM. Samples were prepared utilising the conditions listed in Table 1 and are shown in the ln *J vs.* ln [HF] plot of Fig. 1.

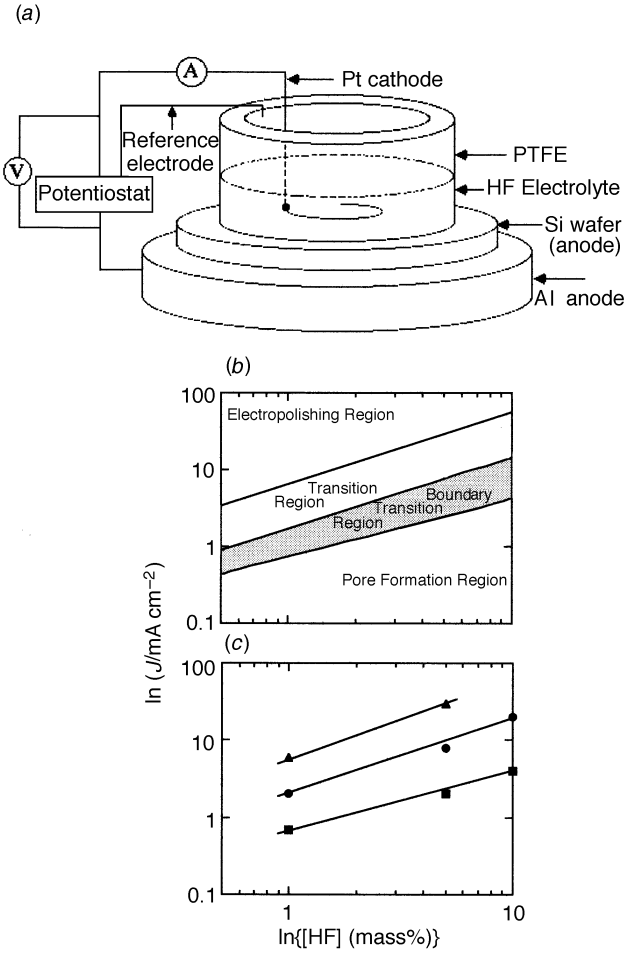

Fig. 1 Anodization cell utilised (*a*); definitions of anodization conditions (*b*); detailed ln *J vs.* ln [HF] plot, showing the boundary transition region conditions utilised (*c*) (▲, sample 1; ●, sample 2; ■, sample 3)

Table 1 Processing conditions

substrate	sample no.	C (%)	J/mA cm^{-1}	t/min	d/μm	X-ray attenuation
n-type Si ⟨111⟩	1	5	5	4	1	1.6
	2	5	10	2	1	2.0
	3	5	2	10	1	1.2
	4	5	20	1	1	1.0
	5	5	5	12	3	2.8
	6	5	5	40	11	3.5
n-Si ⟨000⟩	1	1	5	4	1	1.0
	2	1	2	10	1	2.0
	3	10	10	2	1	2.4
	4	10	20	1	1	2.3
	5	10	50	0.5	1.2	1.0
	6	10	2	10	1	1.0
	7	40	20	5	5	1.0
	8	40	10	5	2.5	1.0
p-Si ⟨100⟩	1	5	5	10	2	1.93
	2	5	7	10	2.5	2.3
	3	5	3	15	1.5	1.0

X-Ray diffraction was carried out on a Siefert 3000 diffractometer utilising Ni-filtered Cu-Kα radiation (λ = 1.5418 Å). Diffraction was examined on the etched part and on adjacent areas of pristine Si for both ⟨100⟩ and ⟨111⟩ faces. Typical raw X-ray measurements are shown in Fig. 2, and Fig. 3 expresses intensity changes with anodization current for several HF concentrations. The coefficient K_A is:

$$K_A = I_o/I_i$$

where I_o = peak intensity of untreated Si surface; I_i = peak intensity after anodization (intensities rather than areas are valid for Si surfaces).

A commercial atomic force microscope (Digital Instruments Nanoscope III) in ambient air conditions was used for monitoring the surface films produced. Images were made by scanning the samples with Si_3N_4 cantilevers having integrated pyramidal tips with spring constants of 0.12 and 0.58 N m^{-1}. The microscope was operated in contact mode and the contact forces between tip and surface were calculated to be *ca.* 30 nN or less. Nanographic images were obtained using a scanner with a maximum operational area of 15×15 μm^2 and micrographs with one having 120×120 μm^2 maximum operational area.

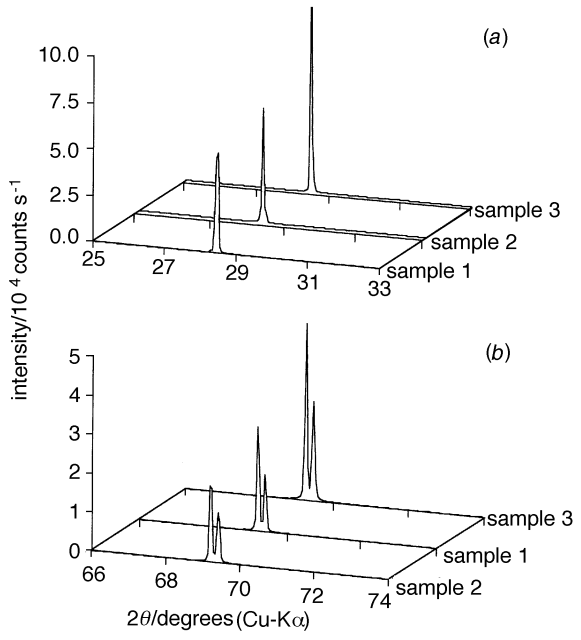

Fig. 2 X-Ray surface diffraction patterns; Si ⟨111⟩ (*a*); Si ⟨100⟩ (*b*)

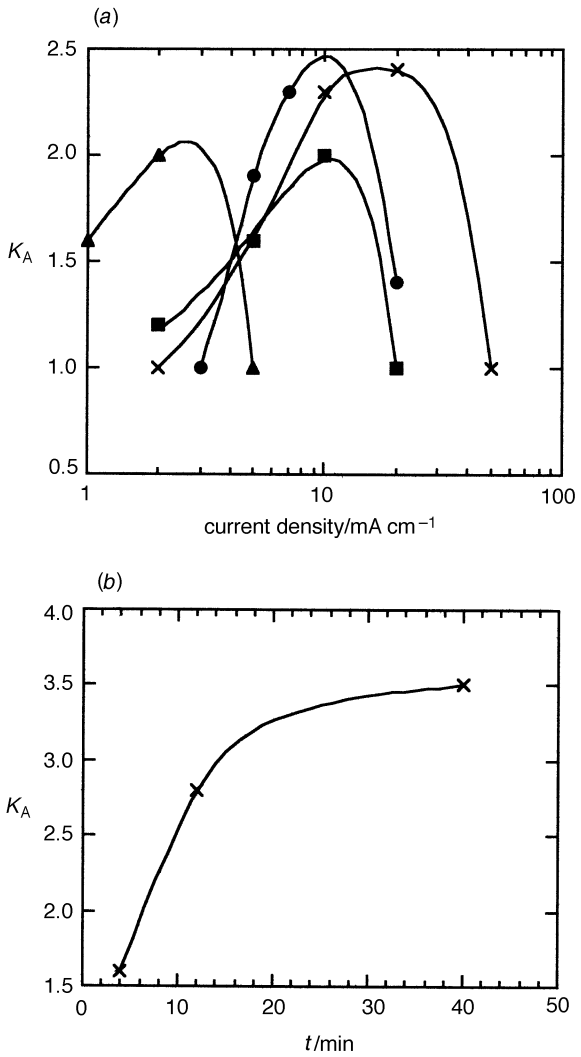

Fig. 3 Changes in X-ray attenuation in Si⟨100⟩ with (*a*) anodisation current (×, 10% ⟨111⟩; ■, 5% ⟨111⟩; ▲, 1% ⟨111⟩; ●, 5% ⟨100⟩) and (*b*) time

Results and Discussion

Initial XRD measurements immediately brought to light significant attenuation of the d_{111} or d_{100} reflections for X-rays incident on the electrolysed area for each type of Si with respect to those on the adjacent unelectrolysed surface (see

Table 2 X-Ray attenuation for n- and p-type Si(111)

sample no.	$\delta/\Omega\ cm^{-1}$	C (%)	$J/mA\ cm^{-1}$	t/min	d/μm	X-ray attenuation
1	n 0.6	1	5	4	1	1.0
2	n 0.6	1	2	10	1	1.1
3	p 4.5	5	5	10	2	1.47
4	p 4.5	1	1.2	25	1	1.0
5	n 0.6	5	5	4	1	1.7

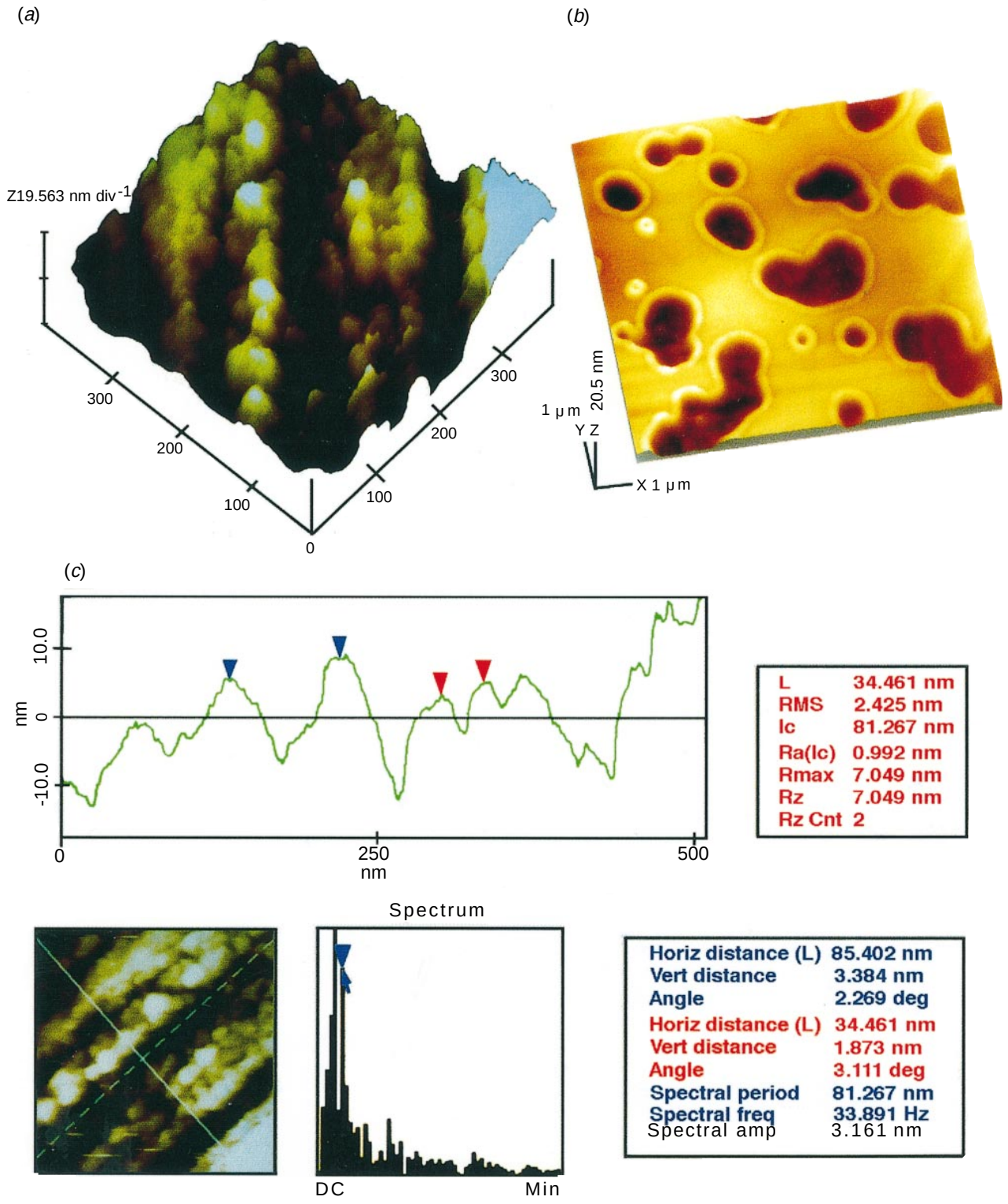

Plate 1 Typical AFM micrograph (dimensions in nm) of the pillared n-Si ⟨111⟩ surface in clinographic projection to underline surface trenches (*a*) and the same sample, cut perpendicular to the ⟨111⟩ face (*b*). (*c*) Section analysis along the white line of the projection (same sample)

Fig. 2, the data correspond to a porous silicon thickness of *ca.* 1 μm). Examination of the points in the topological ln J *vs.* ln [HF] plot of Fig. 1 shows that the effect is observed only for porous silicon films formed in a boundary with the transition regime for porosity (as defined by Zhang *et al.*,[8] and shown as a shaded region in Fig. 1). Both Si ⟨100⟩ and Si ⟨111⟩ surfaces show attenuation, as detailed in Table 2, although most work described below is concerned with Si ⟨111⟩. Further, the effect occurs only for surfaces treated under specific conditions and was found to depend on three factors: (i) the % HF in the electrolysis solution (X-ray absorbance attenuation observed for all HF concentrations less than 10% *m*/*m* in aqueous solution); (ii) the current density; and (iii) the time of electrolysis (which also determines the final film thickness). As shown for Si ⟨111⟩ in Fig. 3, X-ray attenuation reaches a maximum at high HF concentrations.

A typical dependence of K_A on anodization time for Si ⟨100⟩ is also shown in Fig. 3. As expected, the surface becomes increasingly modified as anodization proceeds, the X-ray attenuation effect reaching a maximum after 40 min. In addition, Si ⟨111⟩ appears to more readily form pillar structures and these generally also give higher X-ray attenuation than do those prepared on Si ⟨100⟩.

Further insight into the geometry of the surface arrays formed in the regions of Fig. 1, in particular those responsible for X-ray attenuation, was obtained preliminarily by SEM and subsequently (because there is no need for sample preparation) by AFM. Plate 1 shows a typical AFM micrograph of an n^+ Si ⟨111⟩ surface after 12 min anodization in the boundary transition region. Section analysis of this scan (and many others) shows the presence of pillar-type structures, which are clearly arranged in long trenches and grooves. The more trench-like give relatively flat-topped artefacts, whereas those with more V-shaped grooves have roughly pyramidal structures, as shown in the typical section analysis (Plate 1). For the many micrographs, the final effect is of arrays of both slanted or almost vertical pseudo-planes (see clinographic view in Plate 1). The heights are very variable for both Si ⟨111⟩ and Si ⟨100⟩, but appear not to be higher than *ca.* 50 nm. Further, there is a considerable variation in width, which ranges between 10 and 20 nm. As shown in Plate 2, such arrays are not formed at lower anodization times; the surface appears to be etched randomly with pits of varying cross-sectional geometry and no evidence for the presence of trenches or pseudo-planes could be found. The use of longer anodization times (40 min) gives rise to much deeper etching, with pits often >60 nm in depth (see Plate 2). Vertically cut sections of anodized n^+-Si ⟨111⟩ samples after varying anodisation times gave no X-ray intensity attenuation effects. This suggests that the effect derives from the pseudo-planes described above (and not from any other type of physical effect, such as particular orientations of specific silicon clusters, for example). Finally, inspection of AFM images of n^+-Si ⟨111⟩ sections show the presence of pores of differing dimensions (Plate 1). Many 'embryo' pores are visible with dimensions as low as 5 nm, medium-sized ones having rather V-shaped sections and very large ones (>1 μm) with rounded bottoms. Each is accompanied by a 'rim', which appears to be too ordered to be simply an artefact caused by cutting. As the pores become even larger they coalesce to give kidney-shaped pores, which has been confirmed by SEM studies. These pore geometries are very different from the dendritic pores given by degenerate p-Si[9,10] and also from those of the many anodization conditions in both porous and electropolishing regions investigated previously, which instead give rise to primary and secondary dendritic growth.[11]

First, different levels of impurity, giving rise to preferential etching of either surface, may be discounted as a source of the surface organisation (all samples are from the same Si batch). However, it is well established that etching rates for silicon

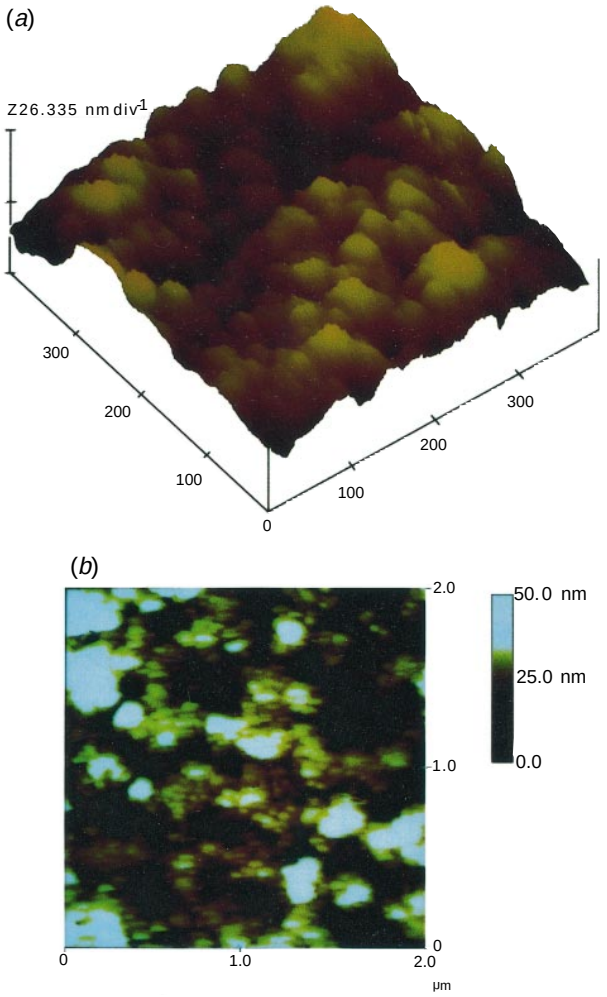

Plate 2 AFM micrographs (dimensions in nm) of n-Si ⟨111⟩ after: 4 min (*a*); 40 min (*b*) anodization

depend on the crystallographic plane under consideration, and follow the order (100)>(110)>(111),[12] that the boundary transition region contains an incoherent silicon oxide film on silicon,[13] and that pit formation implies fast etching at a point.[14] We then suggest that pits are formed first (4 min) which then join laterally after only a few minutes, although the mechanism is as yet obscure. We also note that the samples giving the most developed pseudo-planes (*i.e.* after 12 min) are also those giving the highest photoluminescence effects.

Comparison with recent AFM studies in regions other than the boundary transition region underlines the unique nature of the arrays. For example, Tao *et al.*[14] observed square features on both p- and n-Si surfaces after etching, which they ascribed to the influence of crystallographic factors in pore formation. Conversely, in slightly etched anodized p-Si, You *et al.*[15] detected micropyramids and V-shaped grooves, but no evidence for formation of quantum pillars.

Finally, Plate 3 shows the surface features of a typical Si(111) surface after anodization using conditions in the transition region (see Fig. 1 for definition). Large 'volcano'-like features are observed (diameters 10–20 μm) with relatively small-area, high-surface rough features in fan-like arrangements; in no case did scans show pillar-type arrays or deep pits. It is established that the transition regime for forming porous silicon is characterised by the presence of continuous oxide on the surface,[16] which consists of a variety of forms: $SiO_{0.5}$, SiO, $SiO_{1.5}$. Much work has also been carried out on the dissolution of these species in aqueous HF solution, concluding that higher oxides dissolve faster and that each oxide species shows different behaviour. This provides a rationale for the observed

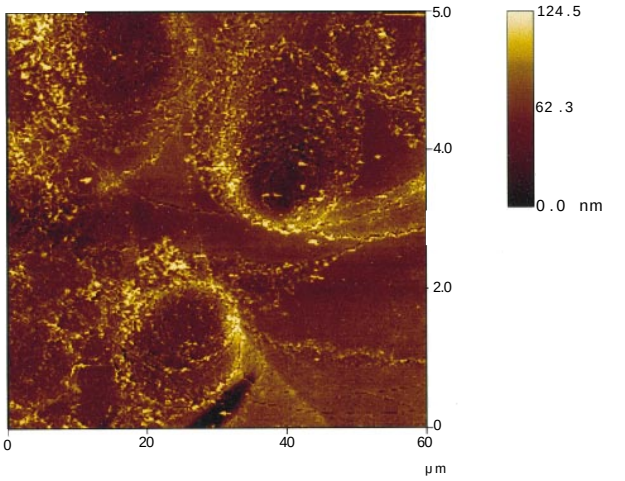

Plate 3 A typical AFM micrograph of Si ⟨111⟩ in the transition region

AFM results: anodization appears to have stripped off a relatively homogeneously thick layer of silicon oxide (the surface is more or less flat after anodization) the rough areas presumably being due to debris left behind by hydrogen bubbles generated during this process. In agreement with this, anodization in the normal regime, *i.e.* when the silicon surface is free of oxide,[3,16] leads to neither a pillar structure nor attenuation effects. The same is the case for porous silicon formed at $>10\%$ HF, because at these concentrations there is no oxide on the porous silicon surface. Further work is under way on inducing formation of more regular arrays in the boundary transition region, correlating them with optical properties and characterising the oxidic species present by FTIR spectroscopy.

Conclusions

Anodization conditions have been found for both p- and n-type silicon which lead to surface arrays of 'pillared' silicon (and silicon oxide) organised in long grooves and trenches. The conditions lie in the boundary transition region of the $\ln J$ *vs.* $\ln[\mathrm{HF}]$ plot. The arrays are obtained in the presence or absence of light stimulation. The boundary transition region conditions apply to various orientations: ⟨100⟩, ⟨110⟩ and ⟨111⟩. The picket-fence arrays so formed cover a very broad range of porous structures, with pillar widths ranging from 20 to 50 Å and inter-pillar porosity with pores >50 Å, as confirmed by AFM imaging.

The materials show anomalous diffraction of X-rays (*e.g.* Cu-Kα, $\lambda = 1.5418$ Å), those conditions giving pillared Si showing intensity reductions of characteristic Si(111) and Si(100) reflections, whereas conditions leading to simple surface-pitted silicon do not show these anomalies.

We thank NATO for a collaborative grant (no. CRG 941174) under the NATO Nanotechnology project, without which this work would not have been possible, Dr. S. Mulley for help with the AFM and Mr. C. Veroli for technical assistance.

References

1 L. T. Canham, *Appl. Phys. Lett*., 1990, **57**, 1046; L. T. Canham, W. Y. Leong, M. I. J. Beale, T. I. Cox and L. T. Taylor, *Appl. Phys. Lett*., 1992, **61**, 2563.
2 S. Lazarouk, V. Bondarenko, P. Pershukevich, S. La Monica, G. Maiello and A. Ferrari, *Mater. Res. Soc. Symp. Proc*., 1995, **358**, 96.
3 R. L. Smith and S. D. Collins, *J. Appl. Phys*., 1992, **71**, R1.
4 R. L. Canham, A. G. Cullis, C. Pickering, O. D. Dosser, T. I. Cox and T. P. Lynch, *Nature (London)*, 1994, **368**, 133.
5 V. P. Bondarenko, A. M. Dorofeev, M. Kazuchits and S. K. Lazarouk, in *Physics, Chemistry and Applications of Nanostructures*, ed. V. Borisenko, S. Gaponenko and S. Gurin, Trans Tech Publications, 1997, in press.
6 S. K. Lazarouk, V. Chumash, E. Fazio, S. La Monica, G. Maiello and E. Proverbio, *Mater. Res. Soc. Symp. Proc*., 1995, **358**, 357; M. Bertolotti, F. Carassiti, E. Fazio, A. Ferrari, S. La Monica and S. Lazarouk, *Thin Solid Films*, 1995, **255**, 365.
7 S. K. Lazarouk and A. A. G. Tomlinson, *Eur. Pat. Appl*., 1996.
8 Q. Zang, S. C. Bayliss and D. A. Hutt, *Appl. Phys. Lett*., 1995, **66**, 1977.
9 V. Lehman, *Adv. Mater*., 1993, **4**, 762.
10 K. Takemoto, Y. Nakamura and O. Nittono, *Jpn. J. Appl. Phys*., 1994, **33**, 6432.
11 V. Lehman and H. Full, *J. Electrochem. Soc*., 1990, **137**, 653.
12 D. L. Kendall, *Ann. Rev. Mater. Sci*., 1979, **9**, 373.
13 P. Allongue, H. Brune and H. Gerischer, *Surf. Sci*., 1992, **275**, 414.
14 Tao Yu, R. Laiho and L. Heikkila, *J. Vac. Sci. Technol. B*, 1994, **12**, 2437.
15 S-L. You, M. Arendt, A. J. Bard, B. Evans, C. Tsai, J. Sarathy and J. C. Campbell, *J. Electrochem. Soc*., 1994, **141**, 402.
16 H. N. Waltenburg and J. Y. Yates, Jr., *Chem. Rev*., 1995, **95**, 1589.

Paper 6/04943E; *Received* 15*th July*, 1996